3-26-2022

Chemical and Carbon Isotopic Characterization of a Karst-Dominated Urbanized Watershed: Case of the Upper San Antonio River

Abongwa T. Pride
Texas A&M University-San Antonio, pabongwa@tamusa.edu

Walter Den
Texas A&M University-San Antonio, wden@tamusa.edu

Aarin Teague
San Antonio River Authority

Chemical and Carbon Isotopic Characterization of a Karst-Dominated Urbanized Watershed: Case of the Upper San Antonio River

Pride T. Abongwa [1,2*], Walter Den[1,2], Aarin Teague[3]

[1]Institute for Water Resources Science and Technology, Texas A&M University-San Antonio, One University Way, San Antonio, Texas 78224, U.S.A.
[2]Department of Mathematical, Physical and Engineering Sciences, Texas A&M University-San Antonio, One University Way, San Antonio, Texas 78224, U.S.A.
[3] San Antonio River Authority, San Antonio, Texas, 78283, U.S.A.

**author of correspondence: pabongwa@tamusa.edu*

Abstract

Urbanization and agriculture are two key factors that place demands on water resources and serve as sources of anthropogenic pollution into inland waterways. The San Antonio River, which is sourced from a karst aquifer, plays an important recreational and scenic role, yet effective management is often hampered by the lack of understanding of the chemical characterization of the water system. The karst-dominated Edwards Aquifer watershed in south-central Texas is an ideal watershed to understand water-rock interaction (carbonate dissolution) and anthropogenic impact on our water resources. In order to understand groundwater-surface water interactions, we made chemical and isotopic measurements over a 17-km stretch of the San Antonio River beginning at the headwater sanctuary and moving downstream. The chemistry of the headwaters and at along the longitudinal profile of the river showed that the Edwards Aquifer is dominated by Ca^{2+}, Mg^{2+} and HCO_3^- ions resulting from carbonate dissolution. The carbon isotopic signature of dissolved inorganic carbon ($\delta^{13}C_{DIC}$) showed that the Edwards Aquifer is in chemical and isotopic equilibrium with soil $CO_{2(g)}$. The relationships between $\delta^{13}C_{DIC}$ and solutes (Cl^-, Na^+, F^-, NO_3^-) showed that anthropogenic sources of these solutes are associated with low $\delta^{13}C_{DIC}$ values,

indicating that carbon isotopic composition of dissolved inorganic carbon can be a useful tracer for contaminants in the environment. The anthropogenic inputs into the San Antonio River were sourced mainly from effluents of the San Antonio Zoo, waste discharge from the River Walk in downtown San Antonio and from fertilizers and animal waste in the less urbanized section of the sampled area (Mission Concepcion to Mission Espada). To protect and sustain the water quality of urban waterways and karst aquifers, urban sewage and effluents must be treated and controlled.

Key words: Karst aquifer, groundwater-surface water interaction, urbanization, carbon isotope, San Antonio River

Introduction

In the U.S., as much as 20% of the land surface is karst and 40% of the groundwater used for domestic supply comes from karst aquifers. Karst formations are composed of soluble carbonate rocks that would dissolve to produce large voids and conduits. These large voids and conduits will make the system susceptible to contamination because of the rapid transport of groundwater through the high-porosity and highly-permeable aquifer material with almost no filtration, sorption, or degradation of dissolved particulate matter (He et al. 2019; White 2018). Karst systems play a critical role in nutrient cycling in the Earth's surface environments and because of the presence of huge solution cavities, they serve as a conduit to the transportation and transformation of heavy metals and other nutrients such as NO_3^- which might pose a serious threat to drinking water supplies in lakes, rivers, springs and streams. In south-central Texas, the Edwards Aquifer is a karst watershed featuring one of the most productive aquifers in the U.S., supporting water supply and agriculture for over 3 million people and 40 rare or endangered species (Edwards Aquifer Authority 2014). The Edwards Aquifer recharges rapidly because its recharge-zone is characterized by the presence of sink-holes and disappearing streams (Sharp and Banner 1997; Opsahl et al. 2018). As a result, the water quality of the Edwards Aquifer is highly susceptible to contamination from nutrients and pesticides derived from anthropogenic sources and has been designated sole-source aquifer (U.S. Environmental Protection Agency 2017a).

The San Antonio River, whose headwater and the upper segment of the river basin passes through a densely populated urbanized area (the City of San Antonio, Texas, USA), overlays the artesian zone of the Edwards Aquifer. Water flows not only in the open channel of a river but also through the interstices of river-channel bank sediments, thus creating a mixing zone with intensified biogeochemical activity with groundwater, referred to as the hyporheic zone (Triska et

al. 1993). The chemistry of the aquifer is influenced by factors such as flow routes and groundwater residence times (e.g., Banner et al. 1996), soil type (e.g., Li et al. 2021), and land use (e.g., He and Wu 2019; He et al. 2020). These will eventually result in groundwater and surface water in some parts of the aquifer to contain higher than normal concentrations of nitrate, chloride, heavy metals and metalloids. The spatial distribution of elevated contaminant levels in groundwater relative to land use will indicate some correspondence between contamination and those parts of the aquifer where urban development has been the heaviest. Conservative tracers such as K, Cl, and stable isotopes of carbon are important proxies that will be used to understand groundwater-surface water interactions (Li et al. 2016a; Zhang et al. 2022). The residence time of water in a drainage basin and the time it is in contact with mineral surfaces is extended after the water first enters a stream, lake, or wetland (Sophocleous 2002). In the case of the Edwards Aquifer, the extended residence time results in the dissolution of the chemically reactive carbonates. The high hydraulic conductivity associated with the Edwards Aquifer transports subsurface flow with physicochemical properties similar to the aquifer materials into the San Antonio River watershed. Therefore, the quality of the river water is profoundly influenced by the dissolved constituents of the aquifer materials. The introduction of high concentrations of Ca^{2+}, Mg^{2+}, and HCO_3^- ions resulting from the dissolution of limestone ($CaCO_3$) and dolomite ($CaMg(CO_3)_2$) could further complicate the identification of possible anthropogenic pollution of the Edwards Aquifer because the type of groundwater discharging into the upper San Antonio River could move from a Ca-HCO_3^- or Ca(Mg)-HCO_3^- type to a Ca-Cl (NO_3^-) or Ca (Mg)-Cl (NO_3^-) type, and Ca-Cl ($+NO_3^- + SO_4^{2-}$) or Ca (Mg)-Cl ($+NO_3- + SO_4^{2-}$) type, indicating anthropogenic-related increases in NO_3^-, Cl^- and SO_4^{2-} concentrations within the watershed (e.g., Jiang et al. 2009). Identifying the sources

and dynamics of water and its constituents within the stream is a key component of managing the resources.

Stable isotopes have become a powerful tool in understanding the biogeochemical processes during groundwater-surface water interaction (Kendall 1998; Cook and Herczeg 2012; Li et al. 2016a; Zhang et al. 2022) complementing conventional physical water quality parameters (pH, temperature, alkalinity, and conductivity) and chemical constituents (inorganic ions). Researchers investigating biogeochemical processes in agro-, groundwater-, and surface-water systems have used stable isotopes of carbon to investigate nutrient flow and capture between systems (Faure 1986; Kendall 1998; Hoefs 2004; Hosono et al. 2009, 2011). Carbon isotope of dissolved inorganic carbon ($\delta^{13}C_{DIC}$) in carbonate species (H_2CO_3, HCO_3^- and CO_3^-) have been used to study carbon evolution and cycling in in-land water systems (Abongwa and Atekwana 2015; Abongwa et al. 2016). It is regarded as a reliable tracer method to reduce the uncertainty when multiple sources of carbon coexist in a water body (Breas et al. 2002), as the isotopic analysis of carbon sources can be a valuable statistical tool for data interpretation, especially when it is examined in combination with the data of other stable isotopes and chemicals (Wen et al. 2020). Therefore, carbon isotope technique have been applied to study the geochemical flux in karstic aquifers (Jackson and Polk 2020), hydrochemical monitoring of urbanized karst water (Wu et al. 2018; Xiao et al. 2020), and the transport of inorganic and biogenic organic carbon across the geochemical boundaries in a karstic aquifer system (Hutchins et al. 2013).

The active hydraulic conductivity also poses a serious threat to the water quality of the aquifer flow when the surface water is being contaminated. For example, in the midst of the rapid urbanization experienced in the San Antonio area, numerous studies have focused on improving the spatial and hydrogeological modeling tool for the assessment of stormwater runoff concerning

rainfall-runoff correlation (El Hassan et al. 2013; Zhao and Gao 2016), nutrients transport (El Hassan et al. 2016) and pathogens distribution (Puri et al. 2009) in various segments of the watershed. Concerning water quality deteriorated by anthropogenic activities, Jiann et al. (2013) reported that the San Antonio River was characterized by high concentrations of ethylenediaminetetraacetic acid, total dissolved phosphate, and suspended matters. More recently, the U.S. Geological Survey performed a seven-year study (2010 to 2016) to better understand how water quality changes under a range of hydrologic conditions and in contrasting land-cover settings (rural and urban) in the San Antonio segment of the Edwards Aquifer (Opsahl et al. 2018) encompassing sampling and analyses of stable isotopes, nutrients, and pesticides covers sampling sites at various sources and sinks. Elevated NO_3^- concentrations showed that the Edwards Aquifer is contaminated by pesticides and its vulnerability is affected by geology and anthropogenic activities within the watershed.

This research focuses on examining the water quality of the intensely urbanized stretch of the San Antonio River, impacting more than 3 billion dollars of tourist industry for the city every year (Nivin 2014). Because of its heavy economic value, the river stretch is also prone to contamination from multiple sources with significant public health implications. . The physical, chemical and isotopic data were collected from both the river and the artesian springs upstream of the watershed. For the purposes of water quality management in urbanized areas in karst terrain, the hydrogeochemical characteristics of the groundwater and surface water was investigated. Specifically, the sources of pollution in the various segments of the urbanized stretch of the San Antonio River were characterized by examining the $\delta^{13}C_{DIC}$ data, combined with the concentration profiles of the metals, alkalinity and nutrients.

Methods

Study Area

Climate, geology, and hydrogeology

The climate of the study area which is located in South Central Texas has a humid subtropical climate. Central Texas is made up of hills and rivers and ranges from semi-arid in the western part to subtropical in the rest (Bhatia et al. 2020). Summers are hot and humid, while winters are mild. Average annual rainfall is in the range of 533 mm in the west to 889mm in the rest of the region. Higher elevations have coniferous tree cover and receive more rainfall than the river valleys that comprise of deciduous trees.

The rocks exposed within the study area are the outcrops of the Trinity and Edwards Groups and the overlying Washita, Eagle Ford, Austin, and Taylor Groups in Hays County. The rocks are sedimentary and formed during the Cretaceous age (Hamilton et al. 2008). The study area is karstic, and characterized by sinkholes, caves, and underground streams that allow rapid infiltration of surface waters to the subsurface. Faulting in the study area is primarily from an Oligocene and early Miocene age extensional fault system known as the Balcones fault zone. The Balcones fault zone generally trends southwest to northeast in southcentral Texas. The faults are vertical to near vertical with normal throw, are en-echelon, and are mostly downthrown to the southeast.

The Edwards Balcones Fault Zone forms the Edwards Aquifer in south-central Texas (Figure 1a) spanning over two million acres in the area. Regional groundwater flow in the aquifer is to the northeast with natural discharge occurring springs and groundwater supply wells. The regional hydrologic conditions are determined by the discharge and geochemistry of the springs and groundwater-supply wells. The hydraulic conductivity transitions from an unconfined,

158 hydrologically-active freshwater system (90-900 cm/d) to confined, basinal brackish water flow
159 (1-2 cm/d) (Sharp 1990), divided by a narrow strip of lithological deformation zone (Figure 1b).
160 The freshwater part (up-dip) is approximately 370 km long from west to northeast and about 16 to
161 65 km wide, bounded to the north by the edge of the recharge zone and to the south and southeast
162 by the downdip limit of freshwater, with only diffuse freshwater flowing across the down-dip
163 (Groschen and Buszka 1997). Several artesian springs along the Edwards Aquifer's discharge zone
164 allow the groundwater to feed into natural streams. The Edwards limestone is between 300-700
165 feet thick, outcrops at the surface in a narrow band, is tilted downward toward the south and east,
166 and is overlain by younger limestone layers and thousands of feet of sediments. Some aquifers,
167 such as those composed of sand or gravel, are relatively uniform throughout and so are
168 called homogenous aquifers. But the Edwards is actually a group of limestones, each with
169 different characteristics, so it is not homogenous at all - it is a highly heterogenic aquifer.
170 Low permeability overlying units are a barrier to vertical flow with upland streams flowing
171 to the south and east, and their watersheds defining the Edwards Aquifer contributing zone (Figure
172 1a). Losses as much as 85% have been recorded as streams crosses the recharge zone, and other
173 contributions to recharge have been via directed and distributed in-stream methods contributing
174 15% - 35% (Slade et al. 1986; Lindgren et al. 2004).
175
176 Sampling locations
177 The study area was an ~17 km stretch of the upper San Antonio River, starting from its
178 headwater – locally known as the Blue Hole (29º28'7.66"N, 98º28'2.76"W), an artesian spring
179 feeding into the San Antonio River – to Mission Espada (29º22'12.46"N, 98º27'26.55"W), as
180 shown in Figures 1 and 2.

Over the sampling distance along the upper San Antonio River, samples were collected at the Brackenridge Park, ~1 km downstream of the Blue Hole and hosts the San Antonio Zoo. At the San Antonio Zoo, about 7.5 million liters of water pumped daily from the Edwards Aquifer is used once for the animals and then discharged into the San Antonio River at Brackenridge Park after ultra-violet disinfection. To focus on the pollution that might originate from the zoo, samples were collected at three different points along the San Antonio River within Brackenridge Park. Samples were also collected along the downtown stretch of the San Antonio River serving as a recreation resource to the local tourism industries. At about 8 km downstream from the Blue Hole, the San Pedro Creek meets the San Antonio River at Mission Concepcion. To understand the pollution sources introduced into main channel of the San Antonio River by the tributary, samples were collected upstream into San Pedro Creek for over 0.5 km. Another sampling location was selected at the outlet of the San Pedro Creek Tunnel, a flood diversion structure with 1.8 km in length further upstream of the San Pedro Creek. The final samples were collected throughout the ~9 km from Mission Concepcion to Mission Espada, a stretch that was a less populated section of the upper San Antonio River.

Sample collections were made during the wet season in the month of June 2019 and the method of sample collection was by grabbing water samples along the flow path of the San Antonio River over a 17 km stretch from the Blue Hole to Mission Espada (Figure 2). The samples were collected during the wet season at a time when the San Antonio River is recharged predominantly by groundwater. Careful consideration was taken such that samples were collected at a period when precipitation had not occurred for about a week so as to minimize rain-water dilution effect. During the dry season, the river water in the San Antonio River is reclaimed water as the groundwater levels are generally too low to recharge the aquifer. All samples were collected on a

204 single day from 8 am to 8 pm on June 14, 2019. The first 14 samples were collected in the more
205 urbanized section of the river over a distance of ~9 km (Blue Hole to Mission Concepcion) and
206 the remaining six samples were collected from a less urbanized area with limited agricultural
207 activity from Mission Concepcion to Mission Espada over the last ~8 km of the sampling distance.
208 The sampling at upstream into San Pedro Creek for ~0.5 km from the San Antonio River-San
209 Pedro Creek confluence was conducted to investigate the potential influence of river dilution on
210 metal evolution within an urbanized watershed.

211 Prior to collecting samples in the field, measurements of temperature, pH and conductivity
212 were made using a Yellow Springs Instrument (YSI, Ohio, USA) multi-parameter probe calibrated
213 to manufacturer's specifications. Water samples collected in the field were filtered through 0.45
214 µm nylon syringe filters. Alkalinity was measured immediately after sampling by acid titration
215 (Hach Company 1992). Samples for anions and cations were collected in high density polyethylene
216 bottles; the cation samples were acidified to a pH <2.0 using high purity HNO_3. Anions (F^-, Cl^-,
217 and NO_3^-) were analyzed using a Dionex Aquion ion chromatograph system (Dionex, California,
218 USA). Cations (Ca^{2+}, Mg^{2+}, K^+ and Na^+) and metals and metalloids (As, Sr and Ba) analyses were
219 conducted following USEPA Method 200.7 (U.S. Environmental Protection Agency 1994), using
220 an Agilent 725 inductively coupled plasma-optical emission spectroscopy (ICP-OES) at the
221 University of Houston's ICP-Analytical Laboratory and Agilent Facility Center.

222 The analyses of stable isotopes of dissolved inorganic carbon (DIC) ($\delta^{13}C_{DIC}$); N from total
223 nitrate ($\delta^{15}N_{NO3-}$); O from total nitrate ($\delta^{18}O_{NO3-}$); H from water (δD_{H2O}); O from water ($\delta^{18}O_{H2O}$)
224 and Sr from water ($\delta^{87}Sr_{H2O}$) were conducted at the Isotope Science Laboratory of the University
225 of Calgary. The stable isotope ratios are reported in the standard delta (δ) notation in per mil (‰):

226 $$\delta(‰) = \left(\left(\frac{R_{sample}}{R_{standard}}\right) - 1\right) \qquad [1]$$

For all isotopic samples, precision and accuracy as 1-sigma of (n=10) was 0.2.

The computer program PHREEQC Version 2.8 (Parkhurst and Appelo 1999) was used to calculate the pCO_2 using pH, temperature and alkalinity and to calculate the temporal equilibrium concentrations in the carbonate species H_2CO_3, HCO_3^- and CO_3^{2-} during carbon evolution. The computer program PHREEQC was also used to calculate the saturation state with respect to calcite using pH, temperature, and alkalinity and Ca^{2+} concentrations.

Results and Discussion

Water quality parameters

The physical and chemical constituents (cations, metals, and anions), carbon isotopic enrichments, and carbonate supersaturation, along the length of the upper San Antonio River studied are plotted in Figure 3. All numerical data corresponding to the sampling locations are compiled in Table 1.

The San Antonio River is in a humid sub-tropical region, and being an urban river, it shows variation (10-40%) in its physical parameters when compared to unperturbed natural streams. The San Antonio River showed substantial variations and characteristics in pH (Figure 3a), alkalinity (Figure 3b) and conductivity (Figure 3c), in its upper-urban channel. For example, the pH slightly fluctuated between 6.99 and 7.28 for the first ~7 km of the sampling distance, and dropped to 6.5 just outside downtown San Antonio (7.33 km). The pH of the San Pedro Creek was generally slightly lower, 7.08 averagely compared to a 7.14 average for the San Antonio River. Beyond the San Antonio River-San Pedro Creek confluence point, the pH dropped from an average of 7.1 to 6.85 for the remainder of the sampling distance (Figure 3a). The alkalinity exhibited a similar pattern, fluctuating between and 249 mg/L 258 mg/L for the first ~8 km. The alkalinity at the San

Pedro Creek sampling sites was significantly lower, averaging 218 mg/L as compared to 253 mg/L for the rest of the samples. Beyond the confluence point, the alkalinity decreased marginally from an average of 253 mg/L to 248 mg/L (Figure 3b).

The conductivity generally showed a steady increase over the sampling length. There was a marked decrease, however, from 845 µS/cm at the Blue Hole to 510 µs/cm immediately downstream (17 m) of the Blue Hole, indicating a rapid loss of dissolved salts when groundwater containing high mineral content discharged into surface water. Additionally, the average conductivity of the San Pedro Creek was recorded at 632 µS/cm, higher than the 592 µS/cm average recorded for the rest of the sampling sites. (Figure 3c). Evidently, the change of these water quality parameters revealed that various streams of water contributed to water flow in the main channel along the sampling length, particular those from the San Pedro Creek. Similar observations also applied to many of the chemical constituents shown in Figures 3d – 3h (cations), Figures 3i – 3j (trace metals), and Figures 3k – 3m (anions). Dissolved carbonates result to a system that shows overall enrichment in $\delta^{13}C$ (Figure 3n), with the accompanying CO_2 exsolution result to supersaturation and calcite precipitation (Figure 3o).

Carbonate dissolution and natural solute contribution

The groundwater chemistry in karst aquifers is controlled by carbonate dissolution, influenced predominantly by the partial pressure of CO_2 (pCO_2), temperature, and pH conditions (Bakalowicz 2005). The positive correlations shown between Ca^{2+} and pCO_2 (Figure 4a) and between $SI_{calcite}$ and pCO_2 (Figure 4b) indicate that the carbonate dissolution, which is closely related to local pCO_2, is responsible for the natural sources of solutes introduced into the Edwards Aquifer and eventually into the upper San Antonio River. The $\delta^{13}C_{DIC}$ detected in the San Antonio River is either introduced through soil CO_2 or from carbonate dissolution. The relationship

exhibited between $\delta^{13}C_{DIC}$ vs. pCO_2 (Figure 4c) was not meaningful (neither strongly positive nor negative correlated), suggesting that the sources of carbon isotopes into the San Antonio River are variable. Calculated saturation indices (SI) showed that the San Antonio River was supersaturated with respect to calcite (Figure 3o), and that the continuous reduction in the concentrations of Ca^{2+} over distance (Figure 3d) was partially caused by the precipitation of calcite on the bed of the San Antonio River that scavenged and sequestered solute Ca^{2+}. The concentrations of Ca^{2+} were weakly correlated with $SI_{calcite}$, showing an $R^2 = 0.032$ (Figure 5a), indicating that while Ca^{2+} was being scavenged from the system by calcite precipitation, the extremely supersaturated state did not show any increasing supersaturation values. The continuous introduction of carbonate species (HCO_3^- and CO_3^{2-}) into the San Antonio River show a somewhat strong correlation with Ca^{2+} (Figure 5b) resulting from the continuous dissolution of carbonate rocks through three parallel reactions (equations 2-4) during rock-water interactions (Plummer et al. 1987; Chou et al. 1989; Wollast 1990):

$$CaMg(CO_3)_2 + 2H^+ \longrightarrow Mg^{2+} + Ca^{2+} + 2HCO_3^- \quad [2]$$

$$CaMg(CO_3)_2 + 2H_2CO_3 \longrightarrow Mg^{2+} + Ca^{2+} + 4HCO_3^- \quad [3]$$

$$CaMg(CO_3)_2 \longrightarrow Mg^{2+} + Ca^{2+} + 2CO_3^{2-} \quad [4]$$

The cations for the San Antonio River can be explained through groundwater – surface water interaction between the Edwards Aquifer and the upper San Antonio River because the aqueous system is dominated by Ca^{2+}, Mg^{2+} and HCO_3^- concentrations.

The Evolution of Sr, Ba and As in the San Antonio River

The impact of water-rock interaction into the overall characterization of the San Antonio River water showed influence of sedimentary rocks by the release of Sr^{2+} and Ba^{2+}. Figures 3h –

297 3j show the concentration profiles of Sr, Ba, and As along the sampling distance. The concentration
298 of the three constituents shared a similar pattern, despite the scale of Sr concentration was one
299 order of magnitude greater than that of Ba and two orders of magnitude greater than that of As.
300 They generally increased over the stretch between the Brackenridge Park and past downtown, and
301 fluctuate at the San Pedro Creek confluence. Different from Sr and Ba, however, As concentration
302 continued to increase over the latter segment of the sampling distance (Figure 3j).

303 Strontium is relatively soluble and common in carbonates groundwater where their
304 occurrence is likely due to the mineralogical substitution of Ca by Sr in the carbonate rocks that
305 make up the Edwards Aquifer (e.g., Musgrove 2002; Musgrove 2021). Sr concentrations ranged
306 from 0.61 to 0.80 mg/L within the upper San Antonio River, with relatively higher concentrations
307 in areas of higher river discharges. Relatively higher river discharges of about 2.2 m^3/s and 2.5
308 m^3/s were recorded in downtown San Antonio (River Walk) and from Mission Concepcion to
309 Mission Espada, respectively. This result indicates that the base flow component of the San
310 Antonio River plays a unique role as higher discharges will release constituents along the river
311 path. Furthermore, the relatively high Sr concentrations in the San Antonio River was observed
312 with neutral pH, as reflected by the carbonate's ability to buffer the system to neutral values. The
313 elevated conductivity of 850 µs/cm at the discharge point indicate a long travel path or
314 groundwater residence time that promotes an extensive water-rock interaction and an elevated Sr
315 in groundwater.

316 Ba concentrations were significantly higher than As throughout the sampling distance, with
317 Ba concentrations ranging from 0.056 mg/L to 0.061 mg/L and As concentrations ranging from
318 0.55 µg/L to 0.93 µg/L (Table 1). The relationship between Ba and As have been reported in wells
319 with higher influence of the marine environment (e.g., Méndez-Rodríguez et al. 2013). Ba is a

biogenic element found in marine sediments in the form of carbonate, and in solution, Ba tends to associate with As at pH 7.47 - 7.66, forming $BaHAsO_4 \cdot H_2O$ and $Ba_3(AsO_4)_2$ (Zhu et al. 2005). The pH of the San Antonio River over the sampling distance ranged from 6.50 to 8.08, providing the physiochemical conditions required to remove As from aqueous solutions. The marine influence on the host rocks of the Edwards Aquifer probably acts as a natural control to help maintain As in a precipitated form, thereby, implying that the Ba-As relationship with the San Antonio River basin results from natural conditions. Sr, Ba and As have similar chemical properties and were correlated along the various zones of the San Antonio River, with relatively higher concentrations at the Blue Hole and from Mission Concepcion to Mission Espada. The concentrations of Sr, Ba, As, and conductivity were highly correlated in the last ~ 10 km of the sampling distance. This observation implies that high evaporation and relatively higher river discharges of 2.5 m^3/s played an important role in balancing their concentrations as the base flow of the river increased the erosive capability and also re-introduced ions into the system.

Na^+, Cl^-, NO_3^- and F^- sources and contribution

The Cl^- concentrations (Figure 3d), showed a marginal increase from 50.4 mg/L to 57.6 mg/L from the first 7.33 km up to the confluence point of the San Antonio River-San Pedro Creek, and remained steady for the remainder of the distance. The average Cl^- concentrations near the San Pedro Creek did not fluctuate as much as other chemical constituents measured. In contrast, as shown in Figures 3l and 3m, both the NO_3^- and F^- concentrations, respectively, showed a continuous decrease over distance. NO_3^-, in particular, decreased sharply from 12.0 mg/L at the Blue Hole to 6.4 mg/L at Mission Espada. Marked concentration fluctuations were once again seen for samples taken near San Pedro Creek confluence.

The equivalent ratio of Cl^-:Na^+ is expected to be 1:1 if those ions are generated solely by the dissolution of evaporite minerals such as halite (Sami 1992; Amantha and Chandrakanta 2014; Li et al. 2016b). Walter et al. (1990) made measurements of 143 samples from the Midwestern United States, and showed that the Cl^-:Na^+ ratio resulting from halite dissolution from ~ 1:1. In this case, we obtained a Cl^-:Na^+ ratio of 5:1, 3:1 and 2:1 from the various stretches of the sampled distance, namely: Blue Hole to confluence point, confluence zone, and the last ~9 km, respectively. Graff et al. (1966) made measurements of 39 samples in the Midwestern Basin of the United States, and had Cl^-:Na^+ ratio of ~2:1, and similar ratios were reported in the sampling zone beyond the Confluence point (i.e., the ~ 9 km of the sampling distance) as stated above. The variations in the Cl^-:Na^+ ratio along the various stretches of the San Antonio River suggests a mixed source contribution of Cl^- and Na^+ into the river. It is suggested that the source of groundwater in the up-dip section of the Edwards Aquifer is an evolved meteoric water: groundwater composition resulting from freshwater interaction with carbonate and evaporite rocks of the Edwards Aquifer (Sharp 1990; Oetting et al. 1996). Cl^- is a conservative ion – one that does not take part in weathering reactions – and it is likely introduced into the natural environment by anthropogenic sources, such as agricultural chemicals (potash or KCl), domestic sewage containing table salts, animal manure, and Cl_2 disinfection treatment of tap water (Sherwood 1989). Panno et al. (2006) collected and made measurements of Na^+ and Cl^- ions from 128 samples mainly from Illinois, United States, and showed that the sources of Na^+ and Cl^- within the basin varied and it is contributed mainly from landfill leachate, septic tank effluent, animal waste and road salts. The relationship between (a) Cl^- and F^-, (b) Cl^- and NO_3^-, and (c) Cl^- and Na^+ are illustrated in Figure 11, which indicates relatively high concentrations of Cl^-, Na^+, NO_3^- and F^- in the San Antonio River. The relatively high concentrations of Cl^- and Na^+ measured could result from both the

366 groundwater (originating from halite dissolution) and from human activities in both residential and
367 agricultural areas of the watershed and these relatively observed increases in Cl^- and Na^+ in the
368 downtown area mirrors the relatively high river discharges of 2.2 m^3/s at the River Walk
369 (downtown). Saline basinal fluids from down-dip section of the aquifer makes its way to the upper
370 section of the San Antonio River via vertical and horizontal pathways of the high-angle normal
371 faults of the Balcones Fault Zone (Oetting et al. 1996). The positive correlation between Cl^- and
372 Na^+ ($R^2 = 0.79$) indicates that they have similar sources, which could be a mixture from evolved
373 groundwater and from domestic sewage that could contain table salts and also predominantly from
374 halite dissolution.

375 The NO_3^- concentrations were relatively high at the headwater sanctuary (Blue Hole) with
376 a concentration of 12.04 mg/L (Table 1) indicating that the major source of contribution of NO_3^-
377 in the San Antonio River is from groundwater recharge. Fertilizers are used commonly in urban
378 and residential landscape, the extent of which is increasing as population grows. There has been a
379 combined population growth of ~ 11% at the upgradient of the regional aquifer flow path (U.S.
380 Census Bureau), which is in line with almost 42,500 kg of N applied over the recharge zone
381 (Turner 2012). Musgrove et al. (2016) determined that the sources of NO_3^- in the contributing and
382 drainage zone of the Edwards Aquifer trended from the boundary between soil NO_3^- and human
383 and animal waste into the human or animal waste NO_3^- field, indicating contribution from both
384 sources. Results from Kendall et al. (2008) showed that denitrification, which is the microbially
385 mediated process of NO_3^- reduction, contributed to low NO_3^- concentrations in stream samples.
386 This potentially accounts for the relatively low NO_3^- concentrations in the last ~10 km of the
387 sampling distance on the San Antonio River and these low concentrations were recorded with
388 relatively high discharge measurements of 2.2 m^3/s at the River Walk (San Antonio Downtown),

389 which further increases to 2.5 m^3/s at Mission Espada (end of sampling distance) as opposed to
390 low discharged measurements of 0.8 m^3/s at the confluence point and 0.43 m^3/s for the San Pedro
391 Creek. The low discharge measurements could indicate that there is less groundwater recharging
392 San Pedro Creek and San Antonio River at the confluence point, thereby resulting in reduced
393 concentrations and increased dilution effect of the constituents, such as NO_3^-. The NO_3^-
394 concentrations dropped from 12.04 to 9.11 mg/L for first 17 m and then increased markedly from
395 9.11 to 11.37 mg/L in Brackenridge Park (Figure 3l). The marked increase in NO_3^- concentration
396 at Brackenridge Park could be attributed to the San Antonio Zoo as the water used within the zoo
397 exhibits is discharged into the San Antonio River, and while treated to remove pathogens via ultra
398 violet disinfection, could contain nutrients from animal manure. The very strong positive
399 relationship exhibited between Cl^- and NO_3^- ($R^2 = 0.78$) indicates a mixed source of NO_3^-, like Cl^-
400 , into the San Antonio River. The trend of F^- concentration across the study area exhibited the same
401 behavior as NO_3^-, showing an overall continuous decrease in concentration throughout the sampled
402 distance (Figure 3m), suggesting that groundwater at the headwater sanctuary of the San Antonio
403 River is the main contributor of F^- into the San Antonio River. While the NO_3^- concentration is
404 attributed mainly to anthropogenic contamination, it is suggested that some of the F^- could
405 originate from natural processes (Farooqi 2007; Young et al. 2010; Li et al. 2019; Liu et al. 2021).
406 The Edwards Aquifer which has saline deposits is characteristic of the inland-sea environments
407 present throughout west Texas during the Permian and Cretaceous Periods, thereby, suggesting a
408 marine source of F^- into the Edwards Aquifer (Hudak 1999). The positive relationship exhibited
409 between Cl^- and F^- ($R^2 = 0.38$) indicates a mixed source of F^-, like Cl^-, into the San Antonio River.
410 This can be attributed to both natural (saline rocks) and anthropogenic sources such as fertilizer
411 use. The negative trends exhibited between Cl^- and F^- (Figure 6a) and Cl^- and NO_3^- (Figure 6b)

412 show that the sources of both NO_3^- and F^- could be similar (anthropogenic), whereas a major source
413 of Cl^- contribution could be from halite dissolution. The positive relationship between Cl^- and Na^+
414 (Figure 6c) show that both ions are sourced from the dissolution of saline rocks that compose the
415 karst matrix of the Edwards Aquifer.
416
417 Carbon isotopic evolution and anthropogenic pollution
418 Figure 3n shows that the $\delta^{13}C_{DIC}$ continuously decreased from -7.96 ‰ to -9.40 ‰ for the
419 first 7.33 km and averages -8.27 ‰ for the San Pedro Creek which was slightly higher than the
420 average of -8.66‰ measured for the San Antonio River before the confluence point. Beyond the
421 confluence point, the $\delta^{13}C$ of the San Antonio River continuously enriched from -9.40 ‰ to -8.48
422 ‰ for the rest of the sampling distance.
423 In carbonate aquifers such as the Edwards Aquifer, the main source of DIC in the
424 groundwater is through carbonate dissolution and soil $CO_{2(g)}$. The measured $\delta^{13}C_{DIC}$ of the water
425 at the headwater sanctuary (Blue Hole) of the San Antonio River was -7.96‰ (Table 1). Soil $CO_{2(g)}$
426 has a $\delta^{13}C$ of about -25‰ (Deines, 1980) with an equilibrium fractionation factor of 7.9‰ at 25
427 ºC (Mook et al. 1974). If the DIC were sourced solely from soil $CO_{2(g)}$, then the water at the Blue
428 Hole should have had a $\delta^{13}C_{DIC}$ of about -18‰. It is reported that the $\delta^{13}C_{DIC}$ of marine and
429 freshwater carbonates can range from -1.5‰ to +2.0‰ (Keith and Weber 1965). Using an
430 equilibrium fractionation factor of 7.9‰ (Mook et al. 1974), a $\delta^{13}C_{DIC}$ of 6.5‰ to 10‰ could be
431 observed at the headwater sanctuary of the San Antonio River. Dandurand et al. (1982) reported a
432 $\delta^{13}C_{DIC}$ of -15‰ from water sourced by a combination of both soil $CO_{2(g)}$ and carbonate dissolution
433 in the unsaturated zone of an aquifer. If it is assumed that the Edwards Aquifer groundwater has
434 equilibrated with soil $CO_{2(g)}$, then with the application of a fractionation factor of 7.9‰ (Mook et

al. 1974) the $\delta^{13}C_{DIC}$ is expected to be around -7.0‰. The dissolution of carbonates and soil respiration to produce HCO_3^- at the measured pH (7-8) will cause kinetic isotopic enrichment in the range of -0.4‰ ±0.2‰ to -3.4‰ ±0.4‰ at 25°C (Turner 1982). The chemical transformation of $CaCO_{3(s)} \rightarrow HCO_3^-{}_{(aq)} \rightarrow CO_{2(aq)}$ will change the isotopic composition of the Edwards Aquifer groundwater to the point of chemical and isotopic equilibrium, such that the resulting carbon isotopic composition of the Edwards Aquifer groundwater at the discharge points of the headwater sanctuary of the San Antonio River (the Blue Hole), will suggest that the DIC in the groundwater is sourced from carbonate rocks and soil $CO_{2(g)}$ (e.g., Kendall et al. 2014). Since the Blue Hole is the headwater source of the San Antonio River, and the isotopic fractionation indicates equilibrium conditions between the soil CO_2 and aquifer materials, it indicates that the San Antonio River is discharged from the up-dip section of the aquifer as shown with the relatively high concentrations of Ca, Mg and HCO_3^- which makes up the carbonate host rock.

The oxidation and decomposition of organic matter releases isotopically light $CO_{2(g)}$, and research has shown that the oxidation of organic matter results in a decrease in $\delta^{13}C_{DIC}$ (Vitoria et al. 2008). Therefore, the $\delta^{13}C_{DIC}$ in rivers that are fed predominantly by groundwater can be a proxy and useful tracer for groundwater pollution sourced from anthropogenic processes. The $\delta^{13}C_{DIC}$ decreased from -7.95‰ at the headwaters to about -8.95‰ at Brackenridge Park where the San Antonio Zoo is housed. The decrease in the $\delta^{13}C_{DIC}$ could result from oxidation and decomposition of organic waste released into the San Antonio River from the zoo. Relatively low $\delta^{13}C_{DIC}$ (-8.61‰ to -9.41‰) were measured at the River Walk, in downtown San Antonio, indicating that increased urban impacts such as stormwater runoff, gasoline leaks, and releases from tour boats within this zone could be introducing organic pollution into the river. The enriched $\delta^{13}C_{DIC}$ values observed for San Pedro Creek (-7.71‰-7.90‰) indicate that there is less organic waste introduced into the

creek than the San Antonio River, as up to this point, the creek travels through concrete tunnels dug in shale-clay layers as a means of flood control within the city of San Antonio. Beyond the San Antonio River-San Pedro Creek confluence point, the $\delta^{13}C_{DIC}$ of the San Antonio River were relatively low ranging from -8.4‰ to -8.95‰, from Mission Concepcion to Mission Espada (final ~9 km of the sampling distance). This represented the section of the San Antonio River with, relatively high flow (~ 2.5 m^3/s); low residential density; and small scale agricultural activity, indicating that fertilizer use and decomposition of organic waste could be responsible for the relatively low $\delta^{13}C_{DIC}$ recorded. Li et al. (2010) showed that groundwater in residential areas with higher anthropogenic sources would produce more negative $\delta^{13}C_{DIC}$ values. High concentrations of NO_3^- produced more negative values of $\delta^{13}C_{DIC}$ especially around the zoo (Figure 7a). The River Walk (downtown San Antonio) with recorded flows of ~2.2 m^3/s and the less urbanized section (from Mission Concepcion to Mission Espada) of the sampling distance characterized by low to high flow from 0.4 m^3/s to 2.5 m^3/s, respectively, show relatively high concentration values of anthropogenic ions. The relationship between $\delta^{13}C_{DIC}$ vs. Cl^- (Figure 7b) shows that water with high concentrations of Cl^- produce more negative values of $\delta^{13}C_{DIC}$, suggesting that Cl^- in the San Antonio River are also sourced partly through anthropogenic activities. A relationship exhibiting a greater negative $\delta^{13}C_{DIC}$ with higher $[Na^+]$ values was observed along the entire stretch of the San Antonio River, although the San Pedro Creek showed a less negative $\delta^{13}C_{DIC}$ vs. high $[Na^+]$ concentration due to the presence of shale-clay beds and concretes over which the San Pedro Creek flows (Figure 7c). The stretch of the San Antonio River from Mission Conception to Mission Espada is dominated by high evaporation as reflected in the relatively higher conductivity values. The relationship between $\delta^{13}C_{DIC}$ and conductivity reflect more negative $\delta^{13}C_{DIC}$ values, indicating that equilibrium fractionation of the carbon isotopes is overshadowed by the more negative values

481 derived from agricultural sources. Additionally, in the upper reaches of the San Antonio River
482 where carbonate concentration is controlled predominantly by groundwater carbonates, the more
483 enriched $\delta^{13}C_{DIC}$ values are due to kinetic fractionation resulting from $CO_{2(g)}$ evasion and from
484 calcite dissolution due to water-rock interaction. Anthropogenic activities can therefore, affect the
485 DIC concentrations in aqueous systems by lowering the $\delta^{13}C_{DIC}$ in groundwater and surface water
486 as evident in these results generated through the Edwards Aquifer – San Antonio River interaction.
487 Since part of the Na^+ in the San Antonio River is derived from the weathering of the host
488 rock (evaporite deposits) and other silicates, it is expected that a strong correlation between Na^+
489 vs. Sr^{2+} is established since Sr is mostly associated with marine carbonates that serve as host rock
490 of the Edwards Aquifer. However, the large variation and weak correlation ($R^2 = 0.09$) between
491 Na^+ vs. Sr^{2+} (Figure 8), suggests a strong anthropogenic input of Na^+ into the San Antonio River,
492 since relatively lower Na^+ values were recorded for the headwater sanctuary of the San Antonio
493 River (9.5 mg/L), indicating that anthropogenic sources of Na^+ into the surface and groundwater
494 of the Edwards Aquifer watershed are not associated with radiogenic Sr in the San Antonio River.
495 The sources of anthropogenic input of Na^+ into the San Antonio River could be from atmospheric
496 deposition and water softeners (e.g., Kelly et al. 2008). Contributions of ions into the San Antonio
497 River are therefore, mostly dual sourced from anthropogenic activities and natural sources (Figure
498 9).
499
500 **Conclusions**
501 The water samples collected from the headwater (Blue Hole) and along the San Antonio
502 River was characterized by relatively high Ca^{2+}, Mg^{2+}, Na^+, Cl^- and NO_3^- concentrations. These
503 ions were combined with $\delta^{13}C_{DIC}$ to evaluate the source of the solutes in this karst watershed. The

504 results showed that the contributions of ions in the watershed are controlled by both natural and
505 anthropogenic processes. While Ca^{2+} and Mg^{2+} were derived from carbonates weathering, Na^{+} and
506 Cl^{-} were sourced both from dissolution of halite beds in the down-dip section of the Edwards
507 Aquifer and from salts discharged from households in the downtown area. The NO_3^{-} concentration
508 was attributed to be sourced through effluent discharge and F^{-} concentrations were sourced through
509 fertilizer use.

510 The relationships between $\delta^{13}C_{DIC}$ vs. solute concentrations exhibited a behavior that
511 suggested that high extents of anthropogenic sources are associated with low $\delta^{13}C_{DIC}$ values. With
512 this, we showed that the relatively high NO_3^{-} concentrations in Brackenridge Park is attributed to
513 the effluent resulting from the San Antonio Zoo, and that the high Cl^{-} concentrations measured at
514 the River Walk (downtown San Antonio) is likely from household waste from business and other
515 effluents introduced into the San Antonio River. Low $\delta^{13}C_{DIC}$ vs. high NO_3^{-} in the less urbanized
516 stretched (Mission Concepcion to Mission Espada) indicated the use of fertilizers, denitrification
517 and animal waste introduction into the San Antonio River.

518 This work showed that the relationship between $\delta^{13}C_{DIC}$ vs. solutes can be used to trace the
519 source of both natural and anthropogenic pollution into an urbanized river. This is a valuable tool
520 for identifying sources of both water and constituents to the stream. By identifying sources of
521 water, water resource managers are able to identify best practices for protecting the quantity and
522 quality of source waters. Furthermore, it provides additional information on the dynamics of
523 constituent fate and transport throughout the groundwater-surface water system. This will
524 contribute to the development of tools, such as modeling and simulation of these systems, to aid
525 stakeholder driven decision processes.
526

Acknowledgments

This research was supported financially by the Research Council Grants (2018-2019 and 2019-2020) and the College of Arts and Sciences' 2019 Summer Grants, Texas A&M University-San Antonio. We thank Samantha Gonzales and Karla Tapia for assisting in the sample collection and analyses. We also thank Dr. Shray Saxena for running the anions samples. Critical reviews by the Associate Editor greatly improved this manuscript.

DECLARATIONS

Ethical Approval

All the authors mentioned in this manuscript have agreed for authorship, read and approved the manuscript, and given consent for submission and subsequent publication of the manuscript.

Consent to Participate

The authors of this research are willing participants of the study.

Consent to Publish

The Authors hereby consents to publication of the Work in any form.

Authors Contributions

The authors: Dr. Pride Abongwa; Dr. Walter Den, and Dr. Aarin Teague conceived the presented idea. Dr. Pride Abongwa, Dr. Walter Den and Dr. Aarin Teague, developed the theory and performed the computations. Dr. Pride Abongwa, Dr. Walter Den and Dr. Aarin Teague verified the analytical methods. Dr. Pride Abongwa, Dr. Walter Den and Dr. Aarin Teague discussed the results and contributed to the final manuscript.

Funding

This research was supported financially by the Research Council Grants (2018-2019 and 2019-2020) and the College of Arts and Sciences' 2019 Summer Grants, Texas A&M University-San Antonio.

Competing Interests

The authors whose names are listed immediately below certify that they have NO affiliations with or involvement in any organization or entity with any financial interest (such as honoraria;

educational grants; participation in speakers' bureaus; membership, employment, consultancies, stock ownership, or other equity interest; and expert testimony or patent-licensing arrangements), in the subject matter or materials discussed in this manuscript.

Availability of Data and Materials

The authors are willing to share and provide the results of the research.

Reference

Abongwa PT, Atekwana EA (2015) Controls on the chemical and isotopic composition of carbonate springs during evolution to saturation with respect to calcite. *Chem. Geol.* 404, 136-149.

Abongwa PT, Atekwana EA, Puckette J (2016) Dissolved inorganic carbon and stable carbon isotopic evolution of neutral mine drainage interacting with atmospheric $CO_{2(g)}$. *Sci. Total Environ.* 545, 57-66.

Anantha RV, Chandrakanta G (2014) Major ion chemistry, hydrogeochemical studies and mapping of variability in ground water quality of Sitanadi basin, Southern Karnataka. *Octa J Environ Res* 2(2):178–196.

Bakalowicz M (2005) Karst groundwater: a challenge for new resources. *Hydrogeol. J.* 13, 148-160.

Banner JL, Musgrove M, Edwards RL, Asmerom Y, Hoff JA (1996) High-resolution temporal record of Holocene groundwater chemistry: Tracing links between climate and hydrology: Geology, v. 24, p. 1049–1052.

Bhatia N, Singh VP, Lee K (2020) Sensitivity of extreme precipitation in Texas to climatic cycles. *Theoretical and Applied Climatology*, pp.1-10.

Breas O, Guillou C, Reniero F, Wada E (2002) The global methane cycle: isotopes and mixing ratios, sources and sinks. *Isot. Environ. Health Stud*. 37 (4), 257-379.

Cook PG, Herczeg AL (2012) Environmental tracers in subsurface hydrology. Springer Science & Business Media.

Chou L., Garrels RM, Wollast R (1989) Comparative study of the kinetics and mechanisms of dissolution of carbonate minerals. *Chem. Geol.* 78, 269-282.

585 Dandurand JL, Gout R, Hoefs J, Menschel G, Schott J, Usdowski E (1982) Kinetically controlled
586 variations of major components and carbon isotopes in a calcite-precipitating spring. *Chem.*
587 *Geol.* 36, 299-315.
588 Deines P, (1980) The isotopic composition of reduced organic carbon, in: Fritz, P., Fontes, J.Ch.
589 Ž. (Eds.) Handbook of Environmental Isotope Geochemistry, 1. The Terrestrial Environment.
590 Elsevier, Amsterdam, pp. 329–406.
591 Edwards Aquifer Authority (2014) Comprehensive Water Management Plan for 2000-2030.
592 Edwards Aquifer Authority.
593 El Hassan AA, Sharif HO, Jackson T, Chintalapudi S (2013) Performance of a conceptual and
594 physically based model in simulating the response of a semi-urbanized watershed in San
595 Antonio, Texas. *Hydrol. Proc.* 27, 3394-3408.
596 El Hassan AA, Xie H, Al-Othman AA, McClelland J, Sharif HO (2016) Water quality modeling
597 in the San Antonio River Basin by radar rainfall data. *Geomat. Nat. Haz. Risk* 7, 953-970.
598 Faure, G., 1986. Principles of Isotope Geology. Wiley, New York, pp. 589.
599 Farooqi A, Masuda H, Kusakabe M, Naseem M, Firdous N (2007) Distribution of highly arsenic
600 and fluoride contaminated groundwater from east Punjab, Pakistan, and the controlling role of
601 anthropogenic pollutants in the natural hydrological cycle. *Geochemical J.* 41, 213-234.
609 Green MG, Wallace WA, (1993) Large diameter tunneling in a soft clay shale-A case history of
610 the San Antonio flood control tunnels, *Int. J. Rock Mech. Min. Sci. Geomech. Abstr.*, 30, 1461-
611 1467.
612 Groschen GE, Buszka PM (1997) *Hydrogeologic framework and geochemistry of the Edwards*
613 *Aquifer saline-water zone, south-central Texas* (Vol. 97, No. 4133). US Department of the
614 Interior, U.S. Geologic Survey.
615 Hach Company (1992) Water Analysis Handbook. Hach Company, Loveland, Co.
616 Hamilton JM, Johnson S, Mireles J, Esquilin R, Burgoon C, Luevano G, Mendoza R (2008)
617 Edwards Aquifer Authority Hydrologic Data Report for 2007. Edwards Aquifer Authority: San
618 Antonio, Texas.
619 He S, Wu J (2019) Relationships of groundwater quality and associated health risks with land
620 use/land cover patterns: a case study in a loess area, northwest China. *Hum. Ecol. Risk Assess.*
621 25(1-2), 354-373.

He X, Wu J, Guo W (2019) Karst spring protection for the sustainable and healthy living: the examples of Niangziguan spring and Shuishentang spring in Shanxi, China. *Expos. Health* 11(2), 153-165.

He S, Li P, Wu J, Elumalai V, Adimalla N (2020) Groundwater quality under land use/land cover changes: A temporal study from 2005 to 2015 in Xi'an, northwest China. *Hum. Ecol. Risk Assess.* 26(10), 2771-2797. 4186

Hoefs J (2004) Isotope fractionation mechanisms of selected elements, in: Stable Isotope Geochemistry, Springer, Berlin, Heidelberg, pp. 31-76.

Hosono T, Wang CH, Umezawa Y, Nakano T, Onodera S, Nagata T, Yoshimizu C, Tayasu I, Taniguchi M. (2011). Multiple isotope (H, O, N, S, and Sr) approach elucidates complex pollutant causes in the shallow groundwaters of Taipei urban area. *J. Hydrol.* 397, 23-36.

Hosono T, Ikawa R, Shimata R, Nakano T, Saito M, Onodera S, Lee KK, Taniguchi M (2009) Human impacts on groundwater flow and contamination deduced by multiple isotopes in Seoul City, South Korea. *Sci. Total Environ.* 407, 3189-3197.

Hutchins BT, Schwartz BF, Engel AS (2013) Environmental control on organic matter production and transport across surface-subsurface and geochemical boundaries in the Edwards Aquifer, Texas, USA. *Acta Carsologica* 42, 245-259.

Hudak PF (1999) Fluoride levels in Texas groundwater. *J. Environ. Sci. Health A.* 34, 1659-1676.

Jackson L, Polk JS (2020) Seasonal delta C-13(DIC) sourcing and geochemical flux in telogenetic epikarst of south-central Kentucky. *Earth Surf. Process Landf.* 45, 785-799.

Jiang Y, Wu Y, Groves C, Yuan D, Kambesis P (2009) Natural and anthropogenic factors affecting the groundwater quality in the Nandong karst underground river system in Yunan, China. *J. Contam. Hydrol. 109*(1-4), 49-61.

Jiann KT, Santschi PH, Presley BJ (2013) Relationship between geochemical parameters (pH, DOC, SPM, EDTA concentration) and trace metal (Cd, Co, Cu, Fe, Mn, Ni, Pb, Zn) concentrations in river waters in Texas (USA). *Aquat. Geochem.* 19, 173-193.

Keith ML, Weber JN (1965) Systematic relationships between carbon and oxygen isotopes in carbonates deposited by modern corals and algae. *Science* 150, 498-501.

Kelly VR, Lovett GM, Weathers KC, Findlay SE, Strayer DL, Burns DJ, Likens GE (2008) Long-term sodium chloride retention in a rural watershed: legacy effects of road salt on stream water concentration. *Env. Sci. Technol. 42*(2), 410-415.

Kendall C (1998) Tracing nitrogen sources and cycling in catchments, in: Isotope Tracers in Catchment Hydrology, pp. 519-576.

Kendall C, Doctor DH, Young MB (2014) Environmental isotope applications in hydrologic studies, in: Holland, H.D., and Turekian, K.K. (eds.), Treatise on geochemistry (2nd ed.).

Kendall C, Elliott EM, Wankel SD (2008) Tracing anthropogenic inputs of nitrogen to ecosystems. RH Michener, K Lajtka (Eds.) Stable Isotopes in Ecology and Environmental Science (2nd ed.), Blackwell Publishing, pp. 375-449.

Li P, Wu J, Qian H (2016a) Preliminary assessment of hydraulic connectivity between river water and shallow groundwater and estimation of their transfer rate during dry season in the Shidi River, China. *Environ. Earth Sci.* 75(2), article 99.

Lindgren RJ, Dutton AR, Hovorka SD, Worthington SRH, Painter S. (2004) U.S. Geological Survey Scientific Investigations Report, 2004–5277.

Li P, Zhang Y, Yang N, Jing L, Yu P (2016b) Major ion chemistry and quality assessment of groundwater in and around a mountainous tourist town of China. *Expos. Health* 8(2), 239-252.

Li P, He X, Li Y, Xiang G (2019) Occurrence and health implication of fluoride in groundwater of loess aquifer in the Chinese Loess Plateau: a case study of Tongchuan, northwest China. *Expos. Health* 11(2), 95-107.

Li XD, Liu CQ, Harue M, Li SL, Liu XL (2010) The use of environmental isotopic (C, Sr, S) and hydrochemical tracers to characterize anthropogenic effects on karst groundwater quality: a case study of the Shuicheng Basin, SW China. *Appl. Geochem.* 25, 1924-1936.

Li Y, Li P, Cui X, He S (2021) Groundwater quality, health risk, and major influencing factors in the lower Beiluo River watershed of northwest China. *Hum. Ecol. Risk Assess.* 27(7), 1987-2013.

Liu L, Wu J, He S, Wang L (2021) Occurrence and distribution of groundwater fluoride and manganese in the Weining Plain (China) and their probabilistic health risk quantification. *Expos. Health* 14, 263–279.

Méndez-Rodríguez L, Zenteno-Savín T, Acosta-Vargas B, Wurl J, Imaz-Lamadrid M (2013) Differences in arsenic, molybdenum, barium, and other physicochemical relationships in groundwater between sites with and without mining activities. *Nat. Sci.* 5, 238-243.

Mook WG, Bommerson JC, Staverman WH (1974) Carbon isotope fractionation between dissolved bicarbonate and gaseous carbon dioxide. *Earth Planet. Sci. Lett.* 22, 169-176.

Musgrove, M., 2021. The occurrence and distribution of strontium in US groundwater. *Appl. Geochem. 126*, 104867.

Musgrove M, Fahlquist L, Houston NA, Lindgren RJ, Ging PB (2010) Geochemical evolution processes and water-quality observations based on results of the National Water-Quality Assessment Program in the San Antonio segment of the Edwards aquifer, 1996–2006: U.S. Geological Survey Scientific Investigations Report 2010-5129.

Musgrove M, Opsahl SP, Mahler BJ, Herrington C, Sample TL, Banta JR (2016) Source, variability, and transformation of nitrate in a regional karst aquifer: Edwards Aquifer, Central Texas. *Sci. Total Environ.* 568, 457-469.

Nivin S. (2014) Impact of the San Antonio River Walk. Study commissioned by the City of San Antonio, San Antonio River Authority, and Paseo del Rio Association.

Oetting GC, Banner JL, Sharp Jr JM (1996) Regional controls on the geochemical evolution of saline groundwaters in the Edwards Aquifer, Central Texas. *J. Hydrol*. 181, 251-283.

Opsahl SP, Musgrove M, Mahler BJ, Lambert RB (2018) Water-quality observations of the San Antonio segment of the Edwards Aquifer, Texas, with an emphasis on processes influencing nutrient and pesticide geochemistry and factors affecting aquifer vulnerability, 2010–16: U.S. Geological Survey Scientific Investigations Report 2018-5060.

Panno SV, Hackley KC, Hwang H., Greenberg SE, Krapac IG, Landsberger S, O'Kelly DJ (2006) Characterization and identification of Na-Cl sources in ground water. *Groundwater*, *44*(2), 176-187.

Parkhurst DL, Appelo CAJ (1999) User's Guide to PHREEQC (Version 2.1)-A Computer Program for Speciation, Batch-Reactions, One-Dimensional Transport and Inverse Geochemical Calculations. U.S. Geological Survey, Water Resource Investigation Report, 99-4256.

Plummer LN, Wigley TML, Parkhurst, DL (1978) The kinetics of calcite dissolution in CO_2-water systems at 5° to 60°C and 0.0 to 1.0 atm CO_2. *Am. J. Sci.* 278, 179-216.

Puri D, Karthikeyan R, Babbar-Sebens M (2009) Predicting the fate and transport of *E. coli* in two Texas rivers basins using a spatially referenced regression model. *J. Am. Water Res. Assoc.* 45, 928-944.

Sami K (1992) Recharge mechanisms and geochemical processes in a semi-arid sedimentary basin, Eastern cape, South Africa. *J. Hydrol.* 139:27–48

Sharp JM, Banner JL (1997) The Edwards Aquifer – A resource in conflict. *Geol. Soc. Am. GSA Today* 7, 1-9.

Sherwood WC 1(989) Chloride loading in the South Fork of the Shenandoah River, Virginia, USA. *Environ. Geol. Water Sci.* 14, 99-106.

Sharp Jr JM (1990) Stratigraphic, geomorphic and structural controls of the Edwards Aquifer, TX, USA, in: E.S. Simpson and J.M. Sharp, Jr. (Eds.), International Association of Hydrogeologists, selected papers for the 28th International Geological Congress, Vol. 1. Heise Hannover, pp. 67-82.

Slade Jr. RM, Dorsey ME, SL S. 1986. U.S. Geological Survey Water-Resources Investigations Report, 86–4036.

Sophocleous M (2002). Interaction between groundwater and surface water: the state of the science. *Hydrogeol. J.* 10, 52-67.

Triska FJ, Duff JH, Avanzino RJ (1993) Patterns of hydrological exchange and nutrient transformation in the hyporheic zone of a gravel-bottom stream: examining terrestrial–aquatic linkages. *Freshw. Biol.* 29, 259-274.

Turner JV (1982) Kinetic fractionation of carbon-13 during calcium carbonate precipitation. *Geochim. Cosmochim. Acta* 46, 1183-1191.

Turner MA (2012) The nitrogen balance of the barton springs segment of the Edwards Aquifer. Changes since Barrett and Charbeneau (1996) Balance. City of Austin Water-shed Protection Department (DR-12-04). (19 p).

United States Environmental Protection Agency (1994) Method 200.7: Determination of metals and trace elements in water and wastes by inductively coupled plasma-atomic emission spectrometry. Revision 4.4. Cincinnati, OH, U.S.A.

U.S. Census Bureau (2014) http://factfinder2.census.gov/faces/nav/jsf/pages/index.xhtml

United States Environmental Protection Agency (2017a) Sole source aquifers for drinking water. Accessed January 2019 at https://www.epa.gov/dwssa.

Vitòria L, Soler A, Canals À, Otero N (2008) Environmental isotopes (N, S, C, O, D) to determine natural attenuation processes in nitrate contaminated waters: example of Osona (NE Spain). *Appl. Geochem.* 23, 3597-3611.

Walter LM, Stueber AM, Huston TJ (1990) Br-Cl-Na systematics in Illinois basin fluids: Constraints on fluid origin and evolution. *Geology, 18*(4), pp.315-318.

746 Wen, Z, Song K, Liu G, Lyu L, Shang Y, Fang C, Du J (2020) Characterizing DOC sources in
747 China's Haihe River basin using spectroscopy and stable carbon isotopes. *Environ. Pollut.* 258,
748 113684.
749 White WB (2018) Contaminant transport in karst aquifers: Systematics and mechanisms, in: White
750 W., Herman, J., Herman, E., Rutigliano, M., (Eds), Karst Groundwater Contamination and
751 Public Health. Advances in Karst Science. Springer, NY, pp 55-81.
752 Wollast R (1990) Rate and mechanism of dissolution of carbonates in the system $CaCO_3$-$MgCO_3$,
753 in: Stumm, W. (Ed.), Aquatic Chemical Kinetics: Reaction Rates of Processes in Natural
754 Waters: New York, J. Wiley & Sons, pp. 431-445.
755 Wu Y, Luo ZH, Luo W, Ma T, Wang YX (2018) Multiple isotope geochemistry and
756 hydrochemical monitoring of karst water in a rapidly urbanized region. *J. Contam. Hydrol.* 218,
757 44-58.
758 Xiao M, Han ZL, Xu S, Wang ZL (2020) Temporal variations of water chemistry in the wet season
759 in a typical urban karst groundwater system in southwest China. *Int. J. Environ. Res. Public*
760 *Health* 17, article 2520.
761 Young, SM, Pitawala A, Ishiga H (2010) Factors controlling fluoride contents of groundwater in
762 north-central and northwestern Sri Lanka. *Env. Earth Sci*. 63, 1333–1342.
763 Zhao G, Gao H (2016) Effects of urbanization and climate change on peak flows over the San
764 Antonio River Basin. *Texas. J. Hydrometeor.* 17, 2371-2389.
765 Zhang L, Li P, He X. (2022) Interactions between surface water and groundwater in selected
766 tributaries of the Wei River (China) revealed by hydrochemistry and stable isotopes. *Hum. Ecol.*
767 *Risk Assess.* 28(1), 79-99.
768

List of Figures:

Figure 1: Map of the USA showing the location of Texas and the Edwards Aquifer (a); map of Texas showing the location of San Antonio (San Antonio River), (b), and a map showing the longitudinal distance of the ~ 17 km sampled stretched of the San Antonio River spanning from the headwater sanctuary - Blue Hole (BLUE HOLE) to Mission Espada (c).

Figure 2: GIS-generated map showing the sampling locations along the urban reach of the San Antonio River, spanning from the headwaters sanctuary to Mission Espada.

Figure 3: Graphs showing the physical, chemical, carbon isotopic ($\delta^{13}C$), and calculated saturated indices of calcite ($SI_{calcite}$) parameters over the sampling distance in the San Antonio River and San Pedro Creek (circled).

Figure 4: Relationships between the partial pressure of $CO_{2(g)}$ (pCO_2) and Ca^{2+} (a), pCO_2 vs. calculated saturation index of calcite ($SI_{calcite}$) (b), and pCO_2 vs. $\delta^{13}C_{DIC}$.

Figure 5: Relationships between the concentrations of, Ca^{2+} vs. $SI_{calcite}$ (a), and Ca^{2+} vs alkalinity (b).

Figure 6: Relationships between the concentrations of Cl^- vs. F^- (a); Cl^- vs. NO_3^- (b), and Cl^- vs. Na^+ (c).

Figure 7: Relationships between $\delta^{13}C_{DIC}$ vs. NO_3^- ions (a); $\delta^{13}C_{DIC}$ vs. Cl^- ions (b), and $\delta^{13}C_{DIC}$ vs. Na^+ ions (c), for the various stretches of the San Antonio River and San Pedro Creek.

Figure 8: Relationship between Na^+ vs. Sr^{2+} ions showing a weak positive correlation between the ions.

Figure 9: Longitudinal display of the San Antonio River from the Blue Hole to Mission Espada, showing the relationship between $\delta^{13}C_{DIC}$ and solutes sources and concentration.

List of Tables:

Table 1: Physical parameters of the ~17-km sampled urban-stretch of the San Antonio River from the Headwater Sanctuary to Mission Espada.

Table 1: Physical, chemical and carbon isotopic ($\delta^{13}C_{DIC}$) parameters of the ~17- km sampled urban-stretch of the San Antonio River from the Headwater Sanctuary to Mission Espada.

Site	Distance km	Latitude N	Longitude W	pH	Alkalinity (mg/L as HCO_3^-)	Conductivity µS/cm	Ca mg/L	K mg/L	Mg mg/L	Na mg/L	As µg/L	Sr mg/L	Ba mg/L	F^- mg/L	Cl^- mg/L	NO_3^- mg/L	$\delta^{13}C_{DIC}$ ‰
Blue Hole (Headwater Sanctuary)	0.00	29°28'7.66"	98°28'2.76"	6.99	258.0	845	55.61	0.90	14.85	9.59	0.55	0.61	0.057	0.78	50.4	12.0	-7.96
University of the Incarnate Word Campus	0.17	29°28'2.32"	98°28'4.06"	7.08	248.4	510	56.68	1.05	14.72	10.29	0.71	0.61	0.058	0.87	48.7	9.1	-8.5
Brackenridge Park (San Antonio Zoo)	0.97	29°27'41.25"	98°28'22.40"	7.23	249.6	540	55.72	1.36	14.89	13.05	0.66	0.64	0.058	0.73	53.0	11.4	-8.45
Brackenridge Park	1.70	29°27'20.12"	98°28'35.12"	7.06	250.8	530	54.54	1.39	14.75	12.98	0.64	0.63	0.057	0.74	53.6	11.5	-8.95
Brackenridge Park	2.24	29°27'4.74"	98°28'44.90"	7.13	258.0	540	55.22	1.42	14.83	13.19	0.62	0.64	0.057	0.7	53.7	11.7	-8.87
Outside of Brackenridge Park	2.80	29°26'47.17"	98°28'51.60"	7.2	255.6	540	53.29	1.42	14.93	13.37	0.63	0.64	0.056	0.69	53.9	11.6	-8.5
Outside Downtown, San Antonio	3.07	29°26'38.18"	98°28'53.61"	7.14	252.0	580	54.73	1.46	15.19	13.81	0.64	0.64	0.058	0.68	39.4	11.3	-8.61
Downtown, San Antonio (River Walk)	5.00	29°25'45.94"	98°29'33.24"	7.16	253.2	580	54.79	1.56	15.58	15.45	0.71	0.67	0.061	0.64	53.3	10.3	-8.6
Downtown, San Antonio (River Walk)	5.37	29°25'31.65"	98°29'31.92"	7.28	249.6	660	54.38	1.61	15.62	15.68	0.72	0.68	0.060	0.66	53.2	10.1	-8.75
Downtown, San Antonio (River Walk)	7.33	29°24'25.13"	98°29'39.53"	6.5	258.0	600	54.86	2.52	15.98	23.62	0.87	0.80	0.060	0.55	57.6	9.5	-9.4
San Pedro Creek (Mission Concepcion)	8.98	29°23'31.41"	98°29'49.37"	7.02	216.0	650	53.20	1.84	15.58	18.14	0.78	0.73	0.060	0.64	55.5	9.7	-8.71
San Pedro Creek (Mission Concepcion)	9.09	29°23'31.86"	98°30'3.25"	7.11	210.0	620	41.92	1.66	14.55	28.64	0.73	0.63	0.054	0.58	53.3	6.3	-7.71
San Antonio River-San Pedro Creek Confluence Point	8.99	29°23'38.52"	98°30'11.96"	7.13	198.0	640	41.44	1.65	14.44	28.15	0.91	0.63	0.056	0.56	53.7	6.2	-8.13
San Antonio River, Mission Concepcion	9.07	29°23'34.86"	98°30'9.51"	7.13	234.0	640	42.35	1.64	14.47	28.68	0.93	0.63	0.055	0.62	53.6	6.3	-7.95
San Antonio River	9.17	29°23'26.23"	98°29'54.64"	7.02	234.0	610	50.94	1.96	15.37	20.74	0.69	0.72	0.059	0.58	55.4	8.8	-8.86
San Antonio River	9.27	29°23'22.86"	98°29'54.79"	6.57	244.8	620	51.11	1.91	15.28	20.09	0.72	0.72	0.059	0.57	55.5	8.9	-8.95
San Antonio River	9.47	29°23'16.25"	98°29'55.73"	6.96	252.0	620	50.90	1.86	15.45	20.38	0.74	0.73	0.060	0.57	55.5	8.7	-8.56
Mission San Jose	10.97	29°22'12.46"	98°28'32.52"	6.93	252.0	630	49.72	1.70	15.19	20.04	0.78	0.68	0.059	0.59	54.6	8.1	-8.67
Mission San Juan Capistrano	14.89	29°20'5.18"	98°27'26.55"	6.96	246.0	640	48.28	1.69	15.27	19.60	0.86	0.69	0.059	0.59	54.3	7.3	-8.6
Mission Espada	16.64	29°19'10.65"	98°26'55.40"	6.9	248.4	640	47.52	1.76	15.18	21.33	0.93	0.68	0.058	0.59	55.2	6.4	-8.48

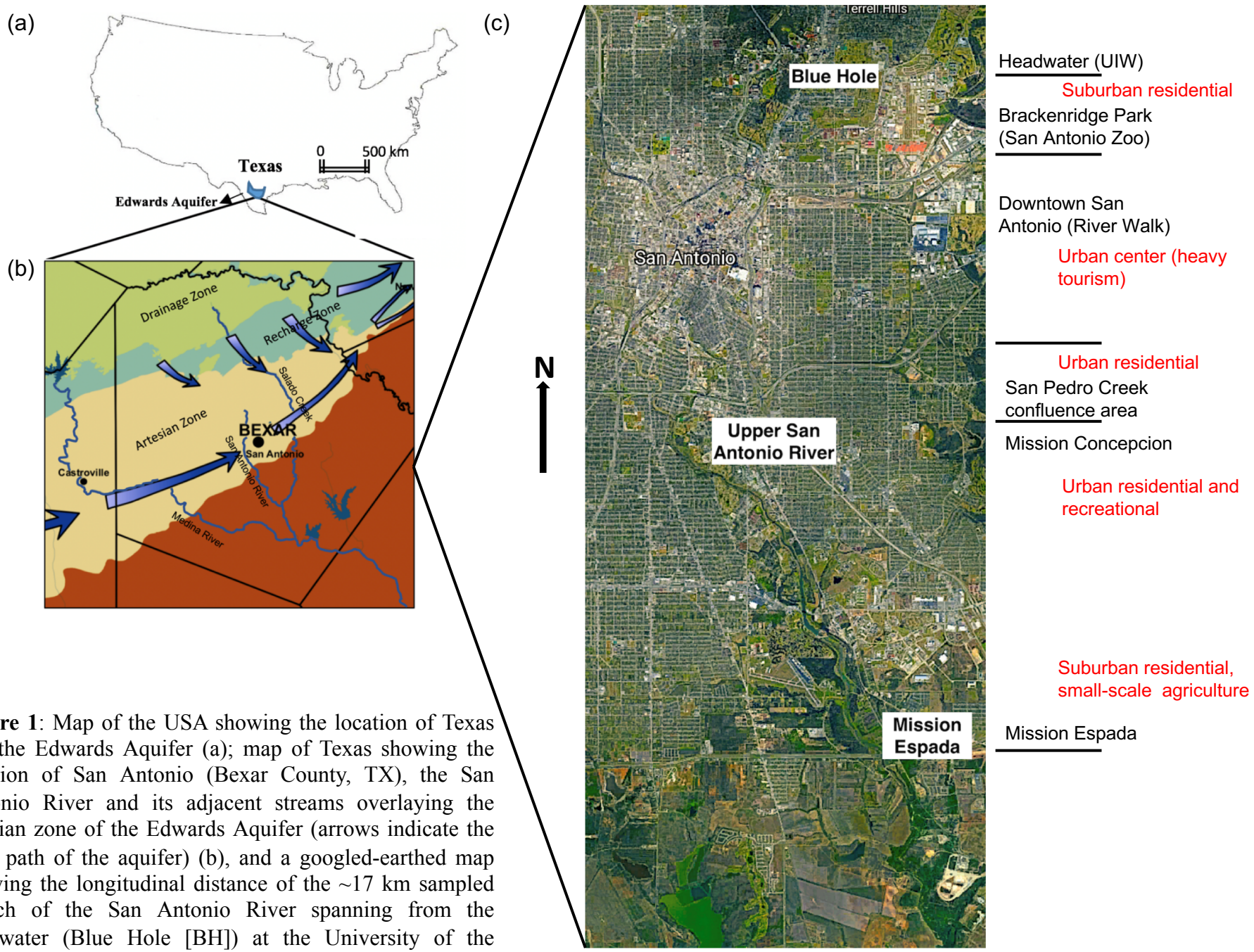

Figure 1: Map of the USA showing the location of Texas and the Edwards Aquifer (a); map of Texas showing the location of San Antonio (Bexar County, TX), the San Antonio River and its adjacent streams overlaying the artesian zone of the Edwards Aquifer (arrows indicate the flow path of the aquifer) (b), and a googled-earthed map showing the longitudinal distance of the ~17 km sampled stretch of the San Antonio River spanning from the headwater (Blue Hole [BH]) at the University of the Incarnate Word [UIW] to Mission Espada (c).

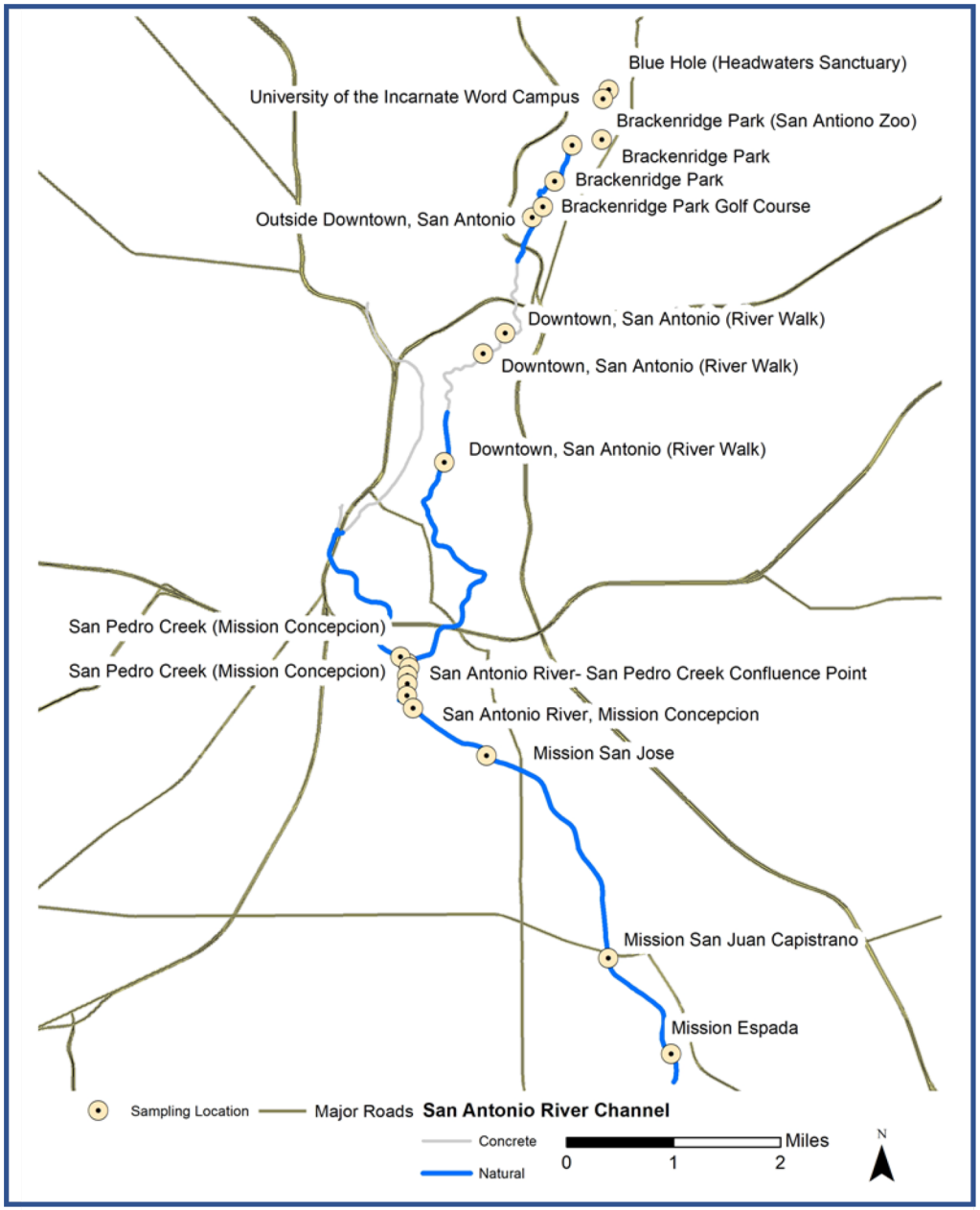

Figure 2: GIS-generated map showing the sampling locations along the urban reach of the San Antonio River, spanning from the headwaters sanctuary to Mission Espada.

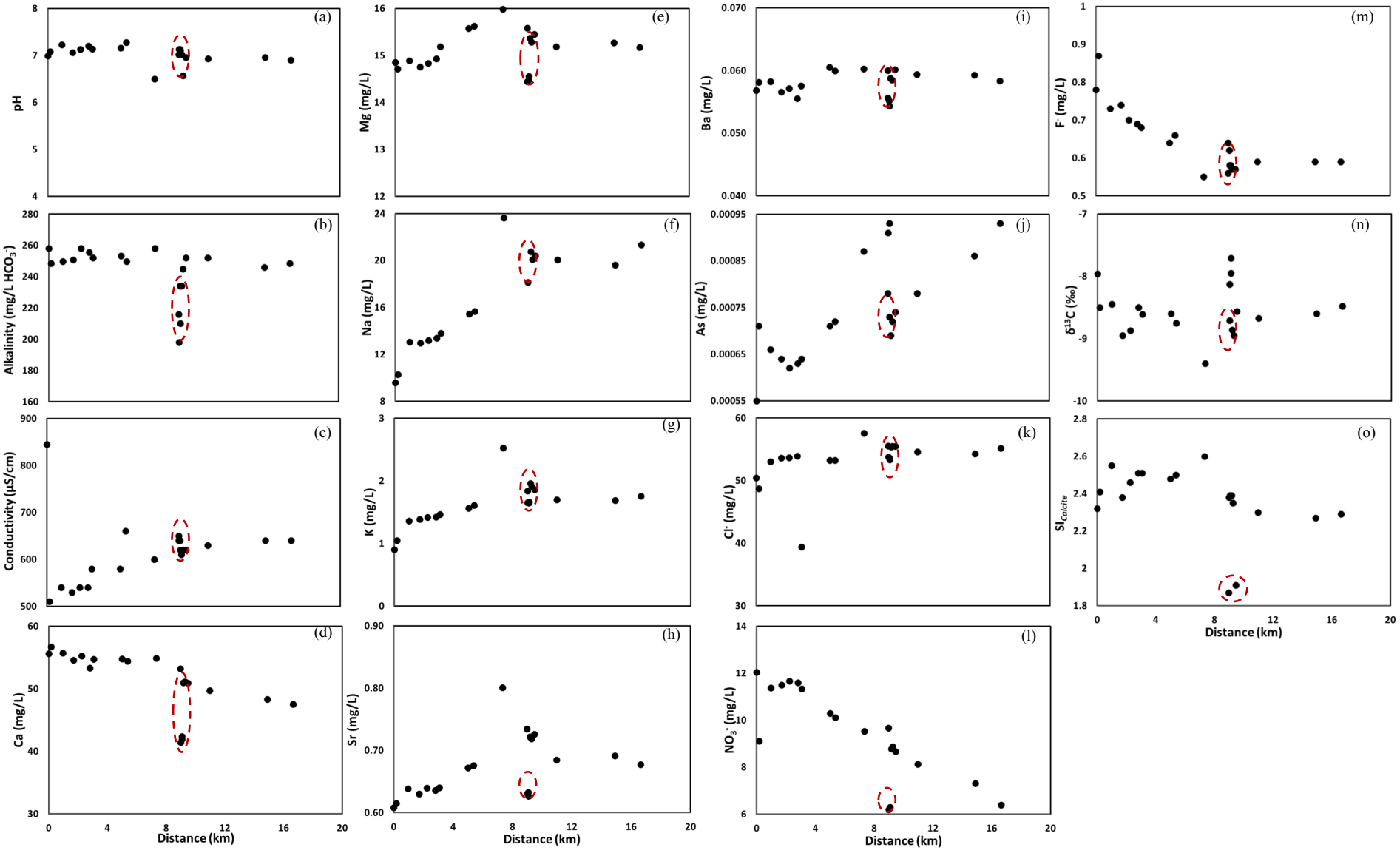

Figure 3: Graphs showing the physical, chemical, carbon isotopic ($\delta^{13}C$), and calculated saturated indices of calcite ($SI_{calcite}$) parameters over the sampling distance in the San Antonio River and San Pedro Creek (circled).

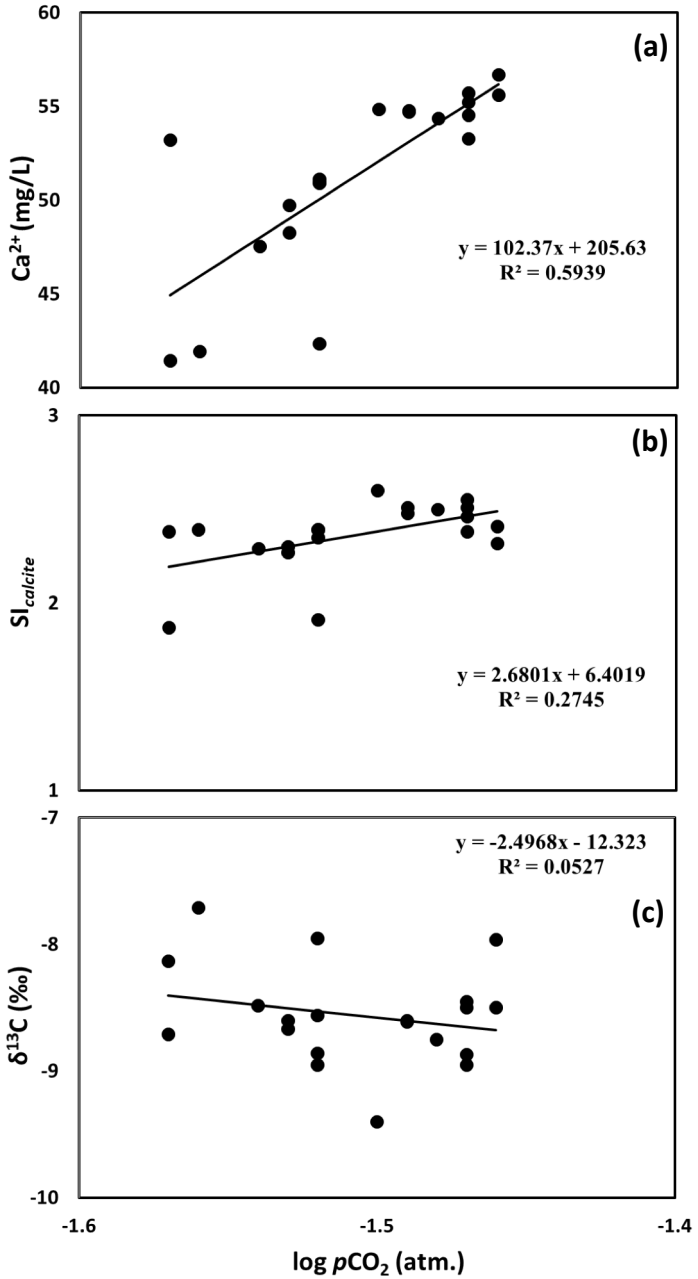

Figure 4: Relationships between the partial pressure of $CO_{2(g)}$ (pCO_2) and Ca^{2+} (a), pCO_2 vs. calculated saturation index of calcite ($SI_{calcite}$) (b), and pCO_2 vs. $\delta^{13}C_{DIC}$

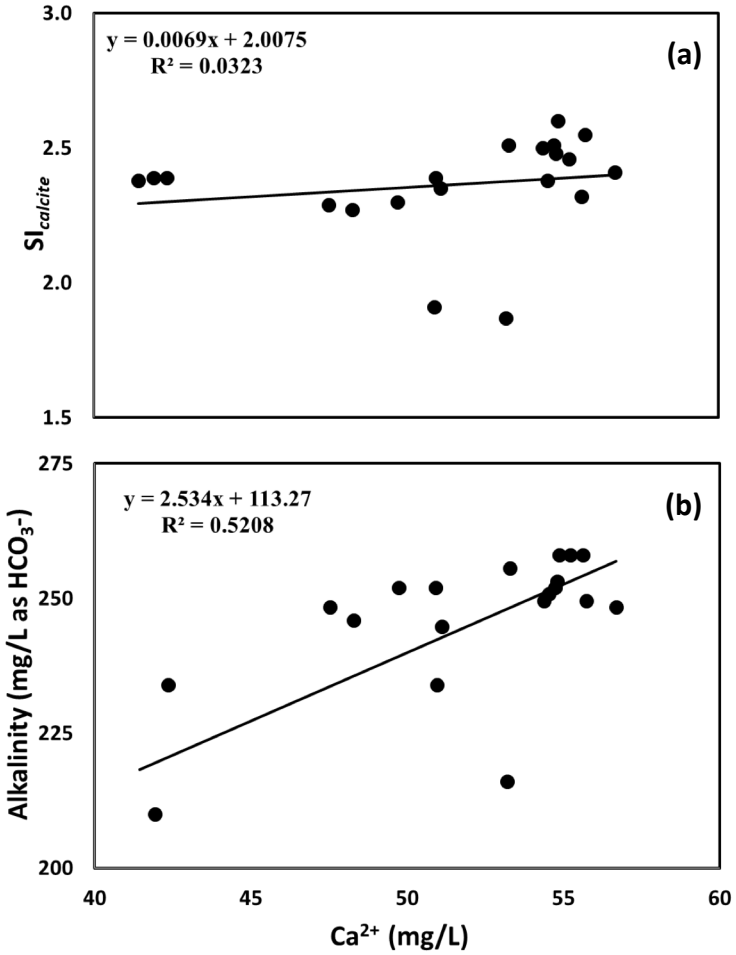

Figure 5: Relationships between the concentrations of, Ca^{2+} vs. $SI_{calcite}$ (a), and Ca^{2+} vs alkalinity (b).

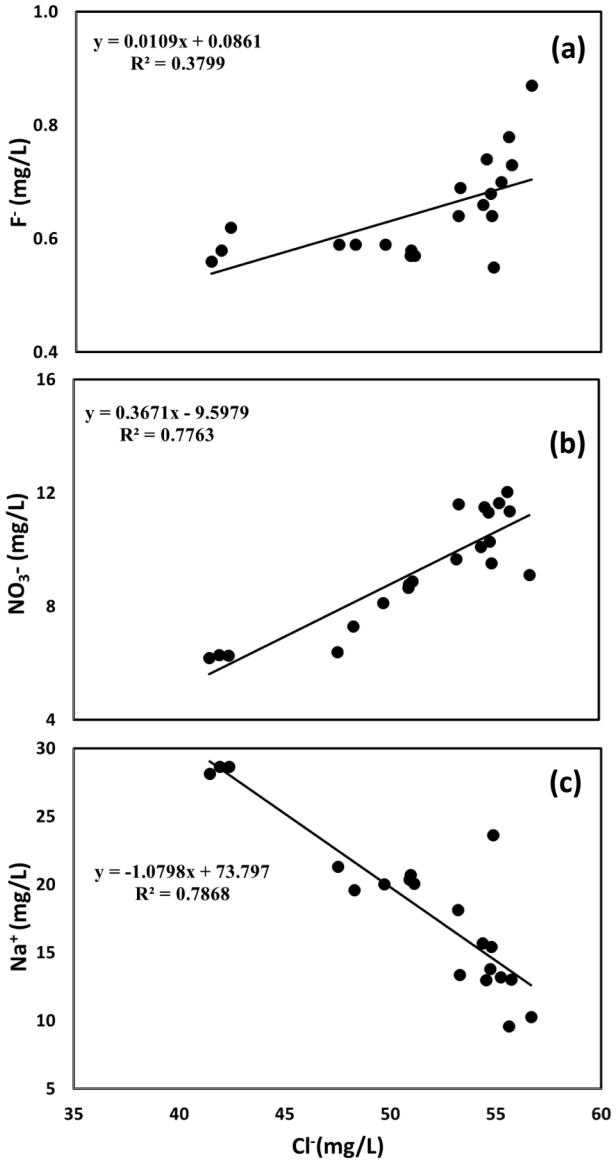

Figure 6: Relationships between the concentrations of Cl^- vs. F^- (a); Cl^- vs. NO_3^- (b), and Cl^- vs. Na^+ (c).

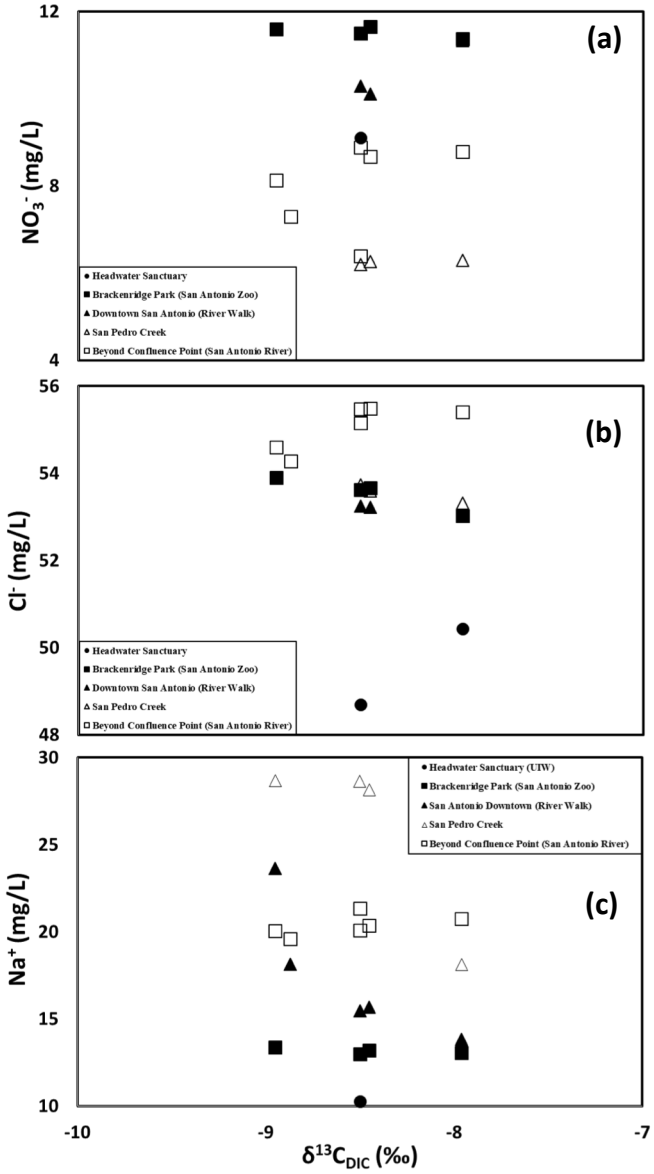

Figure 7: Relationships between $\delta^{13}C_{DIC}$ vs. NO_3^- ions (a); $\delta^{13}C_{DIC}$ vs. Cl^- ions (b), and $\delta^{13}C_{DIC}$ vs. Na^+ ions (c), for the various stretches of the San Antonio River and San Pedro Creek.

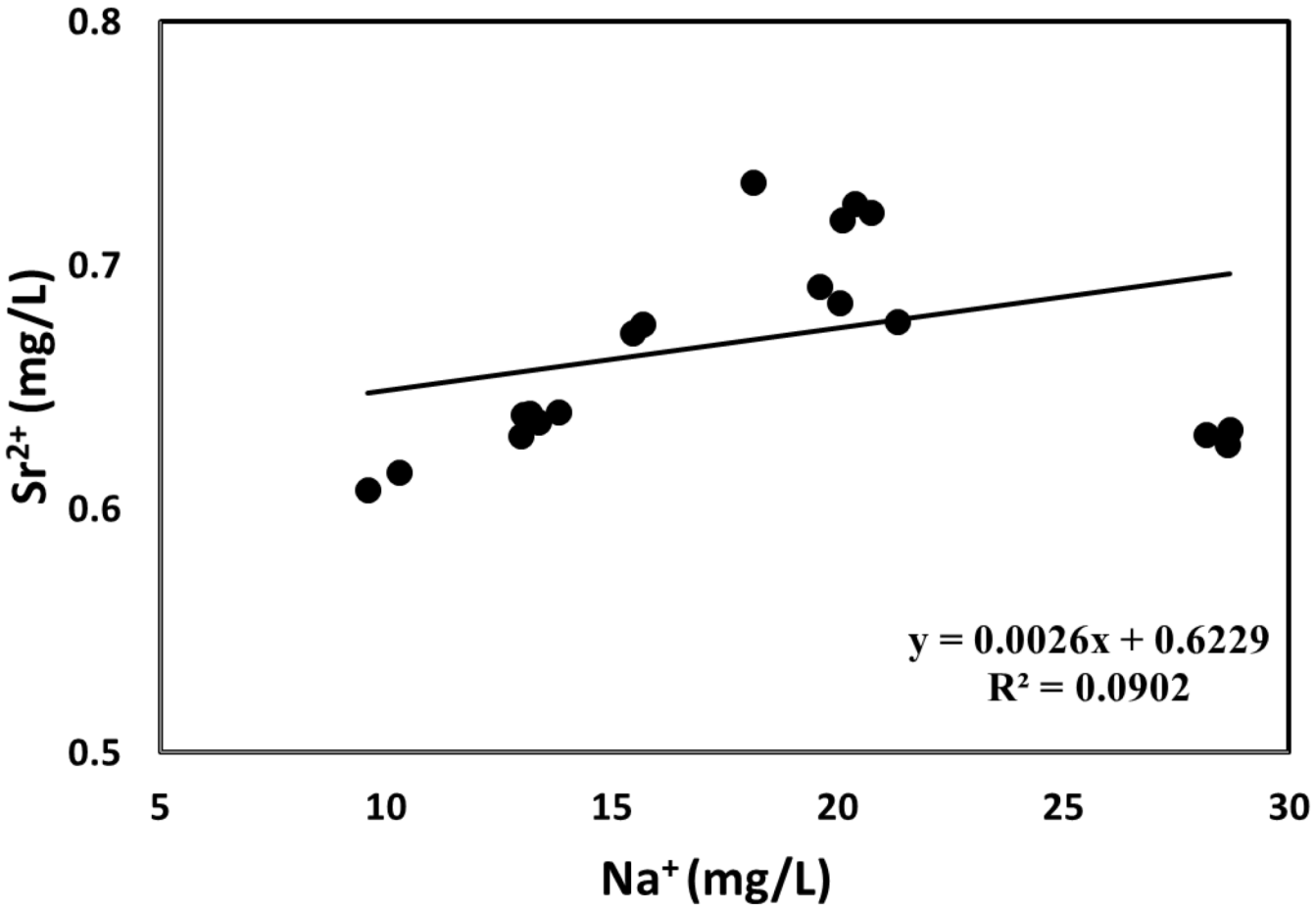

Figure 8: Relationship between Na^+ vs. Sr^{2+} ions showing a weak positive correlation between the ions

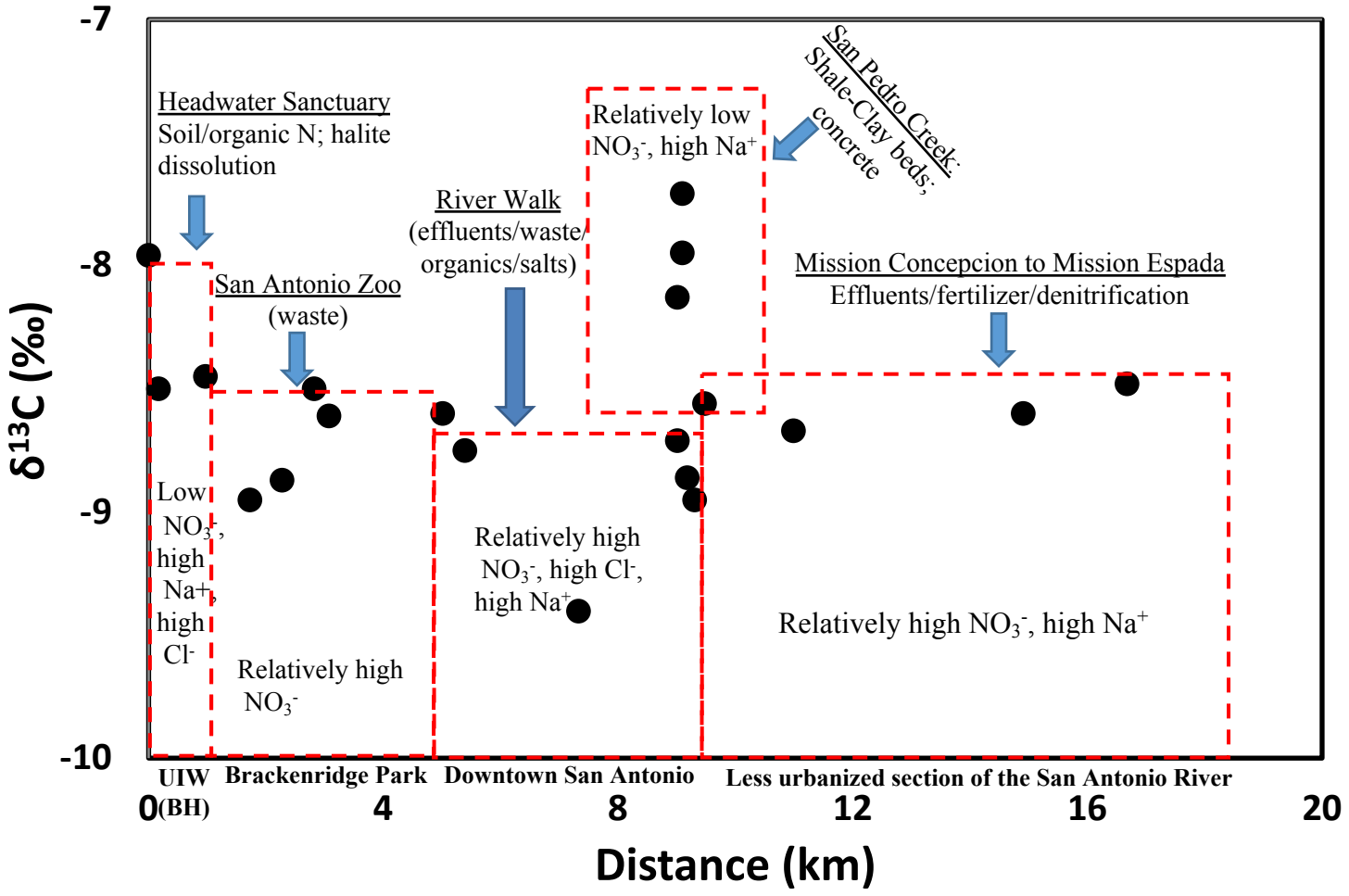

Figure 9: Longitudinal display of the San Antonio River from the headwaters sanctuary at the BH to Mission Espada, showing the relationship between $\delta^{13}C_{DIC}$ and solutes sources and concentration.